The effect of a consistent linearization on the numerical stability of hydrid-elements for quasi-incompressible hyperelastic solids

P. Schneider[1,2,*], J. A. Schönherr[3] and C. Mittelstedt[2]

[1] Deutsches Institut für Kautschuktechnologie e. V. (DIK)
Eupener Straße 33, D-30519 Hannover, Germany
e-mail: patrick.schneider@dikautschuk.de

[2] Institute for Lightweight Construction and Design (KLuB)
Technische Universität Darmstadt
Otto-Berndt-Straße 2, D-64287 Darmstadt, Germany
e-mail: patrick.schneider@klub.tu-darmstadt.de, christian.mittelstedt@klub.tu-darmstadt.de

[3] Center for Structural Materials, State Materials Testing Laboratory (MPA), Institute for Materials Technology (IfW)
Technische Universität Darmstadt
Grafenstraße 2, D-64283 Darmstadt, Germany
e-mail: josef.schoenherr@tu-darmstadt.de

Key words: hybrid finite element, mixed formulation, finite deformation, hyperelasticity, rubber-like material, quasi-incompressible material, discontinuous finite element

Abstract: *We revisit the well-known three-field formulation introduced by Simo and Taylor, [5]. However, while in [5] a semi-discretization is used to eliminate the additional primary unknowns before the problem is linearized in terms of the not yet discretized displacement field, we introduce hybrid/mixed elements based directly on the consistent linearization of the three-field formulation on the continuum-level. In the latter case, static condensation is used to eliminate the additional unknowns on the element-level after the linearization of the continuum formulation in order to derive discontinuous hybrid-elements.*

A family of Simo-Taylor-Pister (`STP`) elements, as well as a family of elements based on the continuum-level linearization (`CL3F`), designed to coincide in terms of the interpolation schemes, the number of assembled degrees of freedom and the number of integration points with the Abaqus hybrid-elements (`C3D8H,C3D20H,C3D10H`) are compared to those elements by benchmark tests. Material parameters were obtained by least-square fitting to experimental data of an industrial NR/IR-blend (natural rubber / isoprene rubber) used for damping applications.

All tested elements are free of volumetric locking. The `STP`-elements show severe stability issues. In general the maximum stable step-width of the Abaqus hybrid-elements is higher in comparison to the `STP`-elements. However, the `CL3F`-elements outperform the Abaqus elements in general without the usage of numerical stabilization. Especially in combination with strongly nonlinear compression models, the advantage of the `CL3F`-elements is huge – here the stable step-width is up to 22 times larger. Details can be found in a contribution which is currently under review, [7].

1 INTRODUCTION

Irreducible (purely displacement-based) finite element formulations are ill-posed for quasi-incompressible materials. In addition, these elements tend to be overly stiff which is an effect known as volumetric locking. To overcome these deficiencies, several so-called mixed and hybrid element formulations were developed. Simo-Taylor-Pister (`STP`) elements were originally introduced in [4, 5] and played a key role in the history of hybrid-element formulations. Usually this formulation is augmented in order to overcome numerical stability issues. Recent hybrid-element formulations often rely heavily on matching numerical stabilization techniques

https://doi.org/10.4995/YIC2021.2021.12174

as well.

2 STP-ELEMENTS

Simo-Taylor-Pister (STP) are based on the modified potential

$$\Pi_{\text{mod}}(\boldsymbol{\varphi}, \Theta, p) \coloneqq \int_\Omega \mathring{W}(\boldsymbol{\varphi}, \Theta)\,\mathrm{d}V + \int_\Omega p\,(J(\boldsymbol{\varphi}) - \Theta)\,\mathrm{d}V + \Pi_{\text{ext}}(\boldsymbol{\varphi}), \tag{1}$$

where the three (primary) unknown tensor fields are: the configuration $\boldsymbol{\varphi}$ (or alternatively the displacement $\boldsymbol{U}$), the dilation Θ and the hydrostatic pressure p. Here $J = \det(\boldsymbol{F})$ denotes the Jacobian and $\mathring{W}$ refers to the modified strain-energy density, where the displacement gradient $\boldsymbol{F}$ is replaced by its modified counterpart $\mathring{\boldsymbol{F}} \coloneqq (\Theta/J)^{1/3}\boldsymbol{F}$. The associated weak form, i.e. Gateaux derivative at the current state $(\hat{\boldsymbol{\varphi}}, \hat{\Theta}, \hat{p})$ in the direction $(\boldsymbol{\eta}, \psi, q)$ (virtual state) is

$$\begin{aligned} G\left(\left(\hat{\boldsymbol{\varphi}}, \hat{\Theta}, \hat{p}\right), (\boldsymbol{\eta}, \psi, q)\right) \coloneqq & \int_\Omega 2\frac{\partial \mathring{W}\left(\hat{\boldsymbol{\varphi}}, \hat{\Theta}\right)}{\partial \mathring{C}_{IJ}} \mathring{\hat{F}}_{iI}\,\mathring{\hat{F}}_{jJ}\,\operatorname{dev}\left(\eta^{\text{sym}}_{i,j}\right)\mathrm{d}V \\ + \int_\Omega \frac{2\psi}{3\hat{\Theta}}\frac{\partial \mathring{W}\left(\hat{\boldsymbol{\varphi}}, \hat{\Theta}\right)}{\partial \mathring{C}_{IJ}} \mathring{\hat{F}}_{iI}\,\mathring{\hat{F}}_{jJ}\,\delta_{ij}\,\mathrm{d}V & + \int_\Omega \hat{p}\,J\left(\hat{\boldsymbol{\varphi}}\right)\eta_{i,i} - \hat{p}\psi + q\left(J\left(\hat{\boldsymbol{\varphi}}\right) - \hat{\Theta}\right)\mathrm{d}V + \delta\Pi_{\text{ext}}(\hat{\boldsymbol{\varphi}}, \boldsymbol{\eta}). \end{aligned} \tag{2}$$

Here, the modified strain-energy density $\mathring{W}$ can still be an arbitrary function of the modified right Cauchy-Green tensor $\mathring{\boldsymbol{C}}$. After the treatment of the weak form, Simo and Taylor assume an additive split of $\mathring{W}$ into an isochoric and volumetric part, cf. [5], section 3.3. The implementation of STP-elements is based on the approach originally sketched in section 4.1 of [5], here referred to as "semi-discretization approach" and recapped below.

The same inter-element discontinuous interpolation for the dilation and the pressure and their virtual counterparts is utilized, using the same shape functions

$${}^{e}\Theta \approx \sum_{l=1}^{{}^{e}n_\Gamma} {}^{e,l}\Gamma(\boldsymbol{\xi})\,\widehat{{}^{e,l}\Theta}, \qquad {}^{e}p \approx \sum_{l=1}^{{}^{e}n_\Gamma} {}^{e,l}\Gamma(\boldsymbol{\xi})\,\widehat{{}^{e,l}p}. \tag{3}$$

Regarding just the additive term of the weak form (2) that incorporates the virtual pressure q and only the contribution of a single finite element ${}^{e}\Omega$, insertion of the interpolations (3) and factoring out the coefficients of the virtual pressure $\widehat{{}^{e,k}q}$ leads to a matrix-vector equation that has to equate to zero. By inversion of the matrix this equation can be solved for the nodal values of the dilation $\widehat{{}^{e,l}\Theta}$, leading finally to an intra-element interpolation for the dilation

$${}^{e}\hat{\Theta} \approx \sum_{k=1}^{{}^{e}n_\Gamma}\sum_{l=1}^{{}^{e}n_\Gamma} {}^{e}H^{-1}_{lk}\int_{{}^{e}\Omega} {}^{e,k}\Gamma(\boldsymbol{\xi})\,{}^{e}J\left(\hat{\boldsymbol{\varphi}}\right)\mathrm{d}V \quad \text{with} \quad {}^{e}H_{kl} \coloneqq \int_{{}^{e}\Omega} {}^{e,k}\Gamma(\boldsymbol{\xi})\,{}^{e,l}\Gamma(\boldsymbol{\xi})\,\mathrm{d}V, \tag{4}$$

that only depends on the current configuration $\hat{\boldsymbol{\varphi}}$. Hence, (4) can be used to eliminate the primary unknown Θ on element level. Applying the same procedure on the additive part of (2) incorporating the virtual dilation ψ, we also obtain an intra-element interpolation for the pressure

$${}^{e}\hat{p} \approx \sum_{k=1}^{{}^{e}n_\Gamma}\sum_{l=1}^{{}^{e}n_\Gamma} {}^{e}H^{-1}_{lk}\int_{{}^{e}\Omega} {}^{e,k}\Gamma(\boldsymbol{\xi})\,\frac{2}{3\hat{\Theta}}\frac{\partial \mathring{W}\left({}^{e}\hat{\boldsymbol{\varphi}}, {}^{e}\hat{\Theta}\right)}{\partial \mathring{C}_{IJ}}\,{}^{e}\mathring{\hat{F}}_{iI}\,{}^{e}\mathring{\hat{F}}_{jJ}\,\delta_{ij}\,\mathrm{d}V, \tag{5}$$

that only depends on the current configuration $\hat{\boldsymbol{\varphi}}$ by the use of (4). The elimination of the independent pressure and the independent dilation in the remainder of (2) by insertion of the intra-element interpolations (4) and (5) leads to a variant of the weak form depending solely on the current configuration $\hat{\boldsymbol{\varphi}}$

$$ {}^{e}g\left(\hat{\boldsymbol{\varphi}},\boldsymbol{\eta}\right) \approx \int_{\boldsymbol{\varphi}({}^{e}\Omega)} \left\{ {}^{e}\hat{\sigma}^{\mathrm{iso}}_{ij} + {}^{e}\hat{p}\,\delta_{ij} \right\} \eta^{\mathrm{sym}}_{i,j}\,\mathrm{d}v + \varphi_{*}\left\{\delta\Pi_{\mathrm{ext}}(\hat{\boldsymbol{\varphi}},\boldsymbol{\eta})\right\}. \tag{6} $$

(Here it is crucial to note that ${}^{e}\hat{p}$ is not the independent pressure anymore, but instead a shorthand notation for the insertion of (5), which also applies for ${}^{e}\hat{\Theta}$ below.) Since (6) only depends on the current configuration $\hat{\boldsymbol{\varphi}}$, i.e. not on the independent dilation and pressure anymore, it can be linearized by derivation of the Gateaux derivative in the direction of the displacement increment $\boldsymbol{u}$ only. The final spatial representation of the linearization reads

$$ \begin{aligned} \delta^{e}g\left(\left(\hat{\boldsymbol{\varphi}},\boldsymbol{\eta}\right),\boldsymbol{u}\right) = \int_{\boldsymbol{\varphi}({}^{e}\Omega)} & u_{i,j}\,{}^{e}\hat{\sigma}_{ij}\eta_{i,l} \\ & + u_{i,j}\eta_{k,l}\left[{}^{e}\hat{p}\left(\delta_{ij}\delta_{kl}-\delta_{il}\delta_{jk}-\delta_{ik}\delta_{jl}\right)+{}^{e}\hat{c}^{\mathrm{iso}}_{ijkl}\right] \\ & + \frac{\partial^{2}\mathring{W}\left({}^{e}\hat{\boldsymbol{\varphi}},{}^{e}\hat{\Theta}\right)}{\partial\Theta^{2}}\,\frac{{}^{e}\hat{\Theta}^{2}}{{}^{e}\hat{J}}\,\overline{\mathrm{div}}\,\boldsymbol{\eta}\,\overline{\mathrm{div}}\,\boldsymbol{u}\,\mathrm{d}v, \end{aligned} \tag{7} $$

where

$$ \overline{\mathrm{div}}\,\boldsymbol{u} = \frac{1}{{}^{e}\hat{\Theta}\left(\hat{\boldsymbol{\varphi}}\right)}\sum_{k=1}^{{}^{e}n_{\Gamma}}\sum_{l=1}^{{}^{e}n_{\Gamma}} {}^{e}H^{-1}_{lk}\int_{{}^{e}\Omega} {}^{e,k}\Gamma(\boldsymbol{\xi})\,{}^{e}J\left(\hat{\boldsymbol{\varphi}}\right)u_{i,i}\,\mathrm{d}V \tag{8} $$

is the so-called "discrete divergence operator", cf. [5]. Finally, the introduction of an inter-element continuous interpolation for the not yet discretized displacement field leads to `STP`-elements. Since only the remaining displacement degrees of freedom are assembled, the implementation is very similar to the procedure for purely displacement-based elements. Due to the used inter-element discontinuous pressure and dilation interpolation (3) `STP`-elements are classified as "discontinuous-type" hybrid elements.

3 CL3F-ELEMENTS

We propose hybrid/mixed elements – closely related to `STP`-elements – we call `CL3F`-elements, which can be of either the discontinuous or the continuous type. A detailed contribution including the full length derivation is currently under review, cf. [7]. The elements are based on the continuum-level linearization of the three-field potentials weak form (2) rather than the semi-discretization approach used for `STP`-elements recapped above.

We assume an isotropic, hyperelastic, quasi-incompressible, material of type

$$ \mathring{W} = \mathring{W}_{\mathrm{iso}}\left(\bar{\mathring{I}}_{1},\bar{\mathring{I}}_{2}\right) + \mathring{W}_{\mathrm{vol}}\left(\Theta\right), \tag{9} $$

where $\bar{\mathring{I}}_{1}$ and $\bar{\mathring{I}}_{2}$ refer to the first two isotropic invariants of $\mathring{\boldsymbol{C}}$. The isochoric and volumetric part of the stress are given by

$$ \sigma^{\mathrm{iso}}_{ij} = 2\,J^{-1}\,\frac{\partial\mathring{W}_{\mathrm{iso}}}{\partial\mathring{C}_{IJ}}\,\mathring{F}_{iI}\,\mathring{F}_{jJ}, \quad \sigma^{\mathrm{vol}}_{ij}(\Theta) = 2\,\Theta^{-1}\,\frac{\partial\mathring{W}_{\mathrm{vol}}}{\partial\mathring{C}_{IJ}}\,\mathring{F}_{iI}\,\mathring{F}_{jJ} = \frac{\partial\mathring{W}_{\mathrm{vol}}}{\partial\Theta}\,\delta_{ij}, \tag{10} $$

and the (isochoric) stiffness is given by

$$ c^{\mathrm{iso}}_{ijkl} = 4\,J^{-1}\,\frac{\partial^{2}\mathring{W}_{\mathrm{iso}}}{\partial\mathring{C}_{IJ}\,\partial\mathring{C}_{KL}}\,\mathring{F}_{iI}\,\mathring{F}_{jJ}\,\mathring{F}_{kK}\,\mathring{F}_{lL}. \tag{11} $$

With (10) and (11) the weak form (2) pushed to the spatial configuration reads

$$\begin{aligned} g\left(\left(\hat{\boldsymbol{\varphi}},\hat{\Theta},\hat{p}\right),(\boldsymbol{\eta},\psi,q)\right) = & \int_{\varphi(\Omega)} \left(\hat{\sigma}^{\text{iso}}_{ij}+\hat{p}\,\delta_{ij}\right)\,\eta^{\text{sym}}_{i,j}\,\mathrm{d}v \\ & + \int_{\varphi(\Omega)} \frac{\psi}{\hat{J}}\left(\frac{1}{3}\,\hat{\sigma}^{\text{vol}}_{ij}\left(\hat{\Theta}\right)\,\delta_{ij}-\hat{p}\right)\mathrm{d}v \\ & + \int_{\varphi(\Omega)} q\left(1-\frac{\hat{\Theta}}{\hat{J}}\right)\mathrm{d}v + \varphi_*\left\{\delta\Pi_{\text{ext}}(\hat{\boldsymbol{\varphi}},\boldsymbol{\eta})\right\}. \end{aligned} \tag{12}$$

Computing the Gateaux derivative of the weak form (2) for a material of type (9) at the current state $(\hat{\boldsymbol{\varphi}},\hat{\Theta},\hat{p})$ in the direction $(\boldsymbol{u},\omega,\gamma)$ (state increment), we obtain the consistent (continuum-level) linearization of the weak form, which reads pushed to the spatial configuration

$$\begin{aligned} & \delta g\Big(\Big((\hat{\boldsymbol{\varphi}},\hat{\Theta},\hat{p}),(\boldsymbol{\eta},\psi,q)\Big),(\boldsymbol{u},\omega,\gamma)\Big) \\ & \quad = \int_{\varphi(\Omega)} \Bigg\{ \hat{c}^{\text{iso}}_{ijkl}\,I^{\text{sym,dev}}_{ijab}\,I^{\text{sym,dev}}_{klcd}\,\eta_{a,b}\,u_{c,d} \\ & \qquad + \hat{\sigma}^{\text{iso}}_{jl}\left(2\,I^{\text{sym,dev}}_{ijab}\,I^{\text{dev}}_{ilcd}-I^{\text{sym,dev}}_{jlad}\delta_{bc}\right)\eta_{a,b}\,u_{c,d} \\ & \qquad + \hat{p}\,\left(\delta_{ab}\,\delta_{cd}-\delta_{cb}\delta_{ad}\right)\eta_{a,b}\,u_{c,d} \\ & \qquad + \frac{\omega\,\psi}{\hat{J}}\,\frac{\partial^2\hat{\mathring{W}}_{\text{vol}}}{\partial\Theta^2}+\gamma\,\eta_{i,i}-\frac{\gamma\,\psi}{\hat{J}}+q\left(u_{i,i}-\frac{\omega}{\hat{J}}\right)\Bigg\}\,\mathrm{d}v \\ & \quad + \varphi_*\left\{\delta\left(\delta\Pi_{\text{ext}}(\hat{\boldsymbol{\varphi}},\boldsymbol{\eta}),\boldsymbol{u}\right)\right\}, \end{aligned} \tag{13}$$

where we introduced

$$\begin{aligned} I^{\text{dev}}_{ijab} &:= \delta_{ia}\delta_{jb}-\frac{1}{3}\delta_{ij}\delta_{ab} && \Rightarrow \text{dev}(t_{ij}) = I^{\text{dev}}_{ijab}\,t_{ab}, \\ I^{\text{sym,dev}}_{ijab} &:= \frac{1}{2}\delta_{ia}\delta_{jb}+\frac{1}{2}\delta_{ib}\delta_{ja}-\frac{1}{3}\delta_{ij}\delta_{ab} && \Rightarrow \text{dev}(t^{\text{sym}}_{ij}) = I^{\text{sym,dev}}_{ijab}\,t_{ab}. \end{aligned}$$

Note that already the mathematical structure of (7) differs from (13): In the STP-linearization the dilation increment ω and pressure increment γ are missing by design, since the independent dilation and pressure variables were removed from the weak form before the linearization. The linearization (7) of the semi-discretization approach used for the STP-elements is not the consistent (continuum-level) linearization of the three-field potentials weak form (2) – it is the consistent linearization of (6).

The linearized problem of finding an incremented equilibrium state is

$$\begin{aligned} 0 &\overset{!}{=} g\left(\left(\hat{\boldsymbol{\varphi}}+\boldsymbol{u},\hat{\Theta}+\omega,\hat{p}+\gamma\right),(\boldsymbol{\eta},\psi,q)\right) \\ &\approx g\left(\left(\hat{\boldsymbol{\varphi}},\hat{\Theta},\hat{p}\right),(\boldsymbol{\eta},\psi,q)\right)+\delta g\Big(\Big((\hat{\boldsymbol{\varphi}},\hat{\Theta},\hat{p}),(\boldsymbol{\eta},\psi,q)\Big),(\boldsymbol{u},\omega,\gamma)\Big). \end{aligned} \tag{14}$$

Choosing the displacement field $\boldsymbol{U}$ as the first primary unknown (rather than the configuration $\boldsymbol{\varphi}$) and introducing a standard Lagrange interpolation

$${}^{e}U_i \approx \sum_{k=1}^{{}^{e}n_k} {}^{e,k}N^i(\boldsymbol{\xi})\,\widehat{{}^{e,k,i}U} \tag{15}$$

for $\boldsymbol{U}$ as well as different (potentially non Lagrange-type) interpolations for the dilation and pressure (3) with matching interpolations for all of the associated virtual quantities $\boldsymbol{\eta}, \psi, q$ and introducing a quadrature scheme for a specific element ${}^e\Omega$, allows us to factor out the nodal values of the virtual quantities as usual to obtain the linear equation system

$$\begin{array}{c} \\ \boldsymbol{\eta}\rightarrow \\ \psi\rightarrow \\ q\rightarrow \end{array} \begin{array}{c} \begin{array}{ccc} \overset{\boldsymbol{u}}{\downarrow} & \overset{\omega}{\downarrow} & \overset{\gamma}{\downarrow} \end{array} \\ \begin{bmatrix} {}^e\boldsymbol{K}_{uu} & \boldsymbol{0} & {}^e\boldsymbol{K}_{up} \\ \boldsymbol{0} & {}^e\boldsymbol{K}_{\Theta\Theta} & {}^e\boldsymbol{K}_{\Theta p} \\ {}^e\boldsymbol{K}_{pu} & {}^e\boldsymbol{K}_{p\Theta} & \boldsymbol{0} \end{bmatrix} \end{array} \cdot \begin{pmatrix} {}^e\boldsymbol{u} \\ {}^e\boldsymbol{\omega} \\ {}^e\boldsymbol{\gamma} \end{pmatrix} + \begin{pmatrix} {}^e\boldsymbol{R}_u - {}^e\boldsymbol{P}_u \\ {}^e\boldsymbol{R}_\Theta \\ {}^e\boldsymbol{R}_p \end{pmatrix} = \boldsymbol{0}, \tag{16}$$

on the element level from (14). By selecting (different) inter-element continuous interpolation schemes (3) and (15), we obtain continuous-type mixed elements by assembling all state variables (displacement, dilation and pressure). Although the element tangent stiffness matrix in (16) is singular (due to the diagonal element which is zero) the global tangent stiffness matrix assembled from (16) is regular.

To obtain discontinuous-type hybrid elements that are comparable to the original `STP`-elements, we choose an inter-element discontinuous interpolation scheme (3) for the dilation and pressure and an inter-element continuous one for the displacement (15). Eliminating the dilation and pressure increments from (16) (static condensation) leads to the equation system

$$\begin{aligned} &\left({}^e\boldsymbol{K}_{uu} + {}^e\boldsymbol{K}_{up}\left[{}^e\boldsymbol{K}_{\Theta p}\right]^{-1}{}^e\boldsymbol{K}_{\Theta\Theta}\left[{}^e\boldsymbol{K}_{p\Theta}\right]^{-1}{}^e\boldsymbol{K}_{pu}\right){}^e\boldsymbol{u} \\ &+{}^e\boldsymbol{R}_u - {}^e\boldsymbol{P}_u + {}^e\boldsymbol{K}_{up}\left[{}^e\boldsymbol{K}_{\Theta p}\right]^{-1}{}^e\boldsymbol{K}_{\Theta\Theta}\left[{}^e\boldsymbol{K}_{p\Theta}\right]^{-1}{}^e\boldsymbol{R}_p - {}^e\boldsymbol{K}_{up}\left[{}^e\boldsymbol{K}_{\Theta p}\right]^{-1}{}^e\boldsymbol{R}_\Theta = \boldsymbol{0}, \end{aligned} \tag{17}$$

$${}^e\boldsymbol{\omega} = -\left[{}^e\boldsymbol{K}_{p\Theta}\right]^{-1}\left({}^e\boldsymbol{K}_{pu}\,{}^e\boldsymbol{u} + {}^e\boldsymbol{R}_p\right), \tag{18}$$

$${}^e\boldsymbol{\gamma} = -\left[{}^e\boldsymbol{K}_{\Theta p}\right]^{-1}\left({}^e\boldsymbol{K}_{\Theta\Theta}\,{}^e\boldsymbol{\omega} + {}^e\boldsymbol{R}_\Theta\right). \tag{19}$$

Only the displacement degrees of freedom (DOFs) are assembled to the global system using the element tangent stiffness contributions and residual vector contributions according to (17). In contrast to the `STP`-approach, the current state values of the independent dilation $\hat{\Theta}$ and the pressure $\hat{p}$ are needed in order to compute the element stiffness and residual vector contributions. Hence, we need to keep track of these quantities, and it is mandatory that every instance of a finite element has internal state variables for the eliminated dilation and pressure DOFs. Once the global equation system – assembled from (17) – is solved, the nodal displacement increments for every element are known and the dilation and pressure increments are computed from (18) and (19) on element level. There is no need for such a secondary variable update scheme in the original `STP`-approach, since – in contrast to the increment-to-increment relations (18) and (19) used in the CL3F-approach – the current states dilation and pressure follow directly from the current displacement, cf. (4) and (5), and thus we have a purely displacement-based approach. The differences in the update schemes are illustrated by the algorithms 1 and 2.

repeat
  assemble $\boldsymbol{K}_T$ from ${}^e\boldsymbol{K}_T\left({}^e\hat{\boldsymbol{U}}, {}^e\hat{\Theta}, {}^e\hat{p}\right)$, cf. (13), (17)
  solve $\boldsymbol{K}_T\boldsymbol{u} = \lambda\boldsymbol{P}_u - \boldsymbol{R}\left(\boldsymbol{R}_u, \boldsymbol{R}_\Theta, \boldsymbol{R}_p\right)$ for $\boldsymbol{u}$, cf. (17)
  foreach element e **do**
    compute ${}^e\omega\left({}^e\boldsymbol{u}\right)$, ${}^e\gamma\left({}^e\boldsymbol{u}\right)$, cf. (18), (19)
    update ${}^e\hat{\Theta} := {}^e\hat{\Theta} + {}^e\omega$, ${}^e\hat{p} := {}^e\hat{p} + {}^e\gamma$
  end
  update $\hat{\boldsymbol{U}} := \hat{\boldsymbol{U}} + \boldsymbol{u}$
  assemble $\boldsymbol{R}$ from ${}^e\boldsymbol{R}_u\left({}^e\hat{\boldsymbol{U}}, {}^e\hat{p}\right)$, ${}^e\boldsymbol{R}_\Theta\left({}^e\hat{\boldsymbol{U}}, {}^e\hat{\Theta}, {}^e\hat{p}\right)$, ${}^e\boldsymbol{R}_p\left({}^e\hat{\boldsymbol{U}}, {}^e\hat{\Theta}\right)$, cf. (12), (17)
until $\|\lambda\boldsymbol{P}_u - \boldsymbol{R}\| \leq \text{tol}$

Algorithm 1: `CL3F` equilibrium iterations at load level $\lambda \in [0, 1]$

repeat
  assemble $\boldsymbol{K}_T$ from ${}^e\boldsymbol{K}_T\left({}^e\hat{\boldsymbol{U}}\right)$, cf. (4), (5), (7)
  solve $\boldsymbol{K}_T\boldsymbol{u} = \lambda\boldsymbol{P}_u - \boldsymbol{R}_u$ for $\boldsymbol{u}$
  update $\hat{\boldsymbol{U}} := \hat{\boldsymbol{U}} + \boldsymbol{u}$
  assemble $\boldsymbol{R}_u$ from ${}^e\boldsymbol{R}_u\left({}^e\hat{\boldsymbol{U}}\right)$, cf. (4), (5), (6)
until $\|\lambda\boldsymbol{P}_u - \boldsymbol{R}_u\| \leq \text{tol}$

Algorithm 2: `STP` equilibrium iterations at load level $\lambda \in [0, 1]$

Since the equation systems of both approaches differ from each other, the discontinuous type `CL3F`-elements differ from the original `STP`-elements, even if we choose the exact same interpolation schemes (3) and (15) in order to achieve a fair comparison. Comparing the equation systems on an element-level, it is interesting to observe that the element residual of the `STP`-approach equals the term ${}^e\boldsymbol{R}_u - {}^e\boldsymbol{P}_u$ in the `CL3F`-approach (compare (6) and the first line of (12)), if we ignore the differences between the pressures in both approaches stemming from the secondary variable update scheme. The additional summands of the vector residual of (17) stemming from ${}^e\boldsymbol{R}_\Theta$ and ${}^e\boldsymbol{R}_p$ are missing in the `STP`-approach due to the semi-discretization. On the other hand, the transformation from the system (17), (19), (18) used by the discontinuous `CL3F`-elements to the discretized consistent linearization (16) (used for the continuous type `CL3F`-elements) is an equivalence transformation on element level.

4 NUMERICAL BENCHMARK

We implemented several types of discontinuous hybrid elements in a finite element program build from scratch following the `CL3F` as well as the original `STP` approach. In order to compare the *formulations* all elements are implemented without extrapolation or any numerical stabilization. We always combine a Lagrange-type displacement interpolation with a polynomial-type dilation/pressure interpolation. The prefixes in the element names below indicate which approach was used. The interpolation schemes are selected to match the ones used for the Abaqus hybrid elements, cf. [6], whose names always start with `C3D` and end with `H`. In turn the number of assembled DOFs coincide. Also the quadrature schemes for `STP` and `CL3F`-elements are selected to match the number of integration points of the Abaqus elements. The Abaqus hybrid elements are used with default parameters, which includes the per default extrapolation.

In particular, we compare the following discontinuous hybrid elements:

- Hexahedral elements with linear Lagrange-type (8 node) displacement interpolation and constant dilation/pressure ansatz, 24 assembled DOFs: `C3D8H`, `STP-H1G8-P0`, `CL3F-H1G8-P0`

- Hexahedral elements with quadratic, serendipity-type Lagrange (20 node) displacement interpolation and linear dilation/pressure ansatz, 60 assembled DOFs: `C3D20H`, `STP-H2sG27-P1`, `CL3F-H2sG27-P1`

- Tetrahedral elements with quadratic Lagrange-type (10 node) displacement interpolation and constant dilation/pressure ansatz, 30 assembled DOFs: `C3D10H`, `STP-T2G4-P0`, `CL3F-T2G4-P0`

Also we implemented the following continuous type `CL3F`-elements for a comparison:

- `CL3F-H2sG27-L1`: A hexahedral element with quadratic, serendipity-type Lagrange (20 node) displacement interpolation and linear Lagrange-type (8 node) dilation/pressure ansatz, 76 assembled DOFs

- `CL3F-T2G4-L1`: A tetrahedral element with quadratic Lagrange-type (10 node) displacement interpolation and linear Lagrange-type (4 node) dilation/pressure ansatz, 38 assembled DOFs

To benchmark the influence of the strength of the nonlinearity in the material model, we combine the Neo-Hooke model for the isochoric part of the strain energy density ($\mu_0 = 1.0316\,\mathrm{MPa}$) with three different compression models. Sorted by the strength of the uplift from weakest to strongest nonlinearity, the compression models are:

- Ogden compression model, cf. [2], $\mathring{W}_{\mathrm{vol}} = \frac{K_0}{\beta^2}\left(\beta \ln \Theta + \Theta^{-\beta} - 1\right)$, $K_0 = 2781$ MPa, $\beta = -2$

- Standard compression model, $\mathring{W}_{\mathrm{vol}} = \frac{1}{2} K_0 \left(\Theta - 1\right)^2$, $K_0 = 2816$ MPa

- Hartmann-Neff model, cf. [1], $\mathring{W}_{\mathrm{vol}} = \frac{K_0}{2\beta^2}\left(\Theta^{\beta} + \Theta^{-\beta} - 2\right)$, $K_0 = 2290$ MPa, $\beta = 41$

All compression models are (least-square) fitted to the same experimental data obtained by confined axial compression testing of an industrial NR/IR-blend (natural rubber / isoprene rubber) with strongly nonlinear compression behavior used for damping applications, cf. [3].

The benchmark geometry, boundary conditions and the load-case are adapted from the well known block locking test, described in detail in [8, pp. 458].

Standard tests for finite element performance are usually mesh convergence studies: To asses an elements stiffness, the load-case is fixed and the mesh is refined in several steps towards the point where the solution does not change anymore within a certain tolerance. Usually one plots the maximum displacement vs. the mesh size for illustration. For each of the three groups of comparable discontinuous hybrid elements (and for each compression model), we see the same mesh convergence behavior. Here we only provide the plot for quadratic hexahedral elements for brevity, cf. Figure 1. The displacements fields coincide beside small round-off errors for different, comparable elements – even in the regime where the displacement is still mesh dependent. Especially all tested discontinuous elements are free of volumetric locking, like the original `STP`-elements, judged by the displacement-field. The continuous `CL3F`-elements have a different mesh convergence behavior, if compared to discontinuous elements with the same displacement ansatz. They need a slightly finer mesh to converge, but still the elements are free of volumetric locking. Their convergence is non-monotonic in contrast to the discontinuous elements. Also it is noteworthy that each equilibrium iteration is computationally more expensive than for comparable discontinuous elements due to the increased number of DOFs for a fixed mesh size. These disadvantages are however to some extent counterbalanced by the fact that

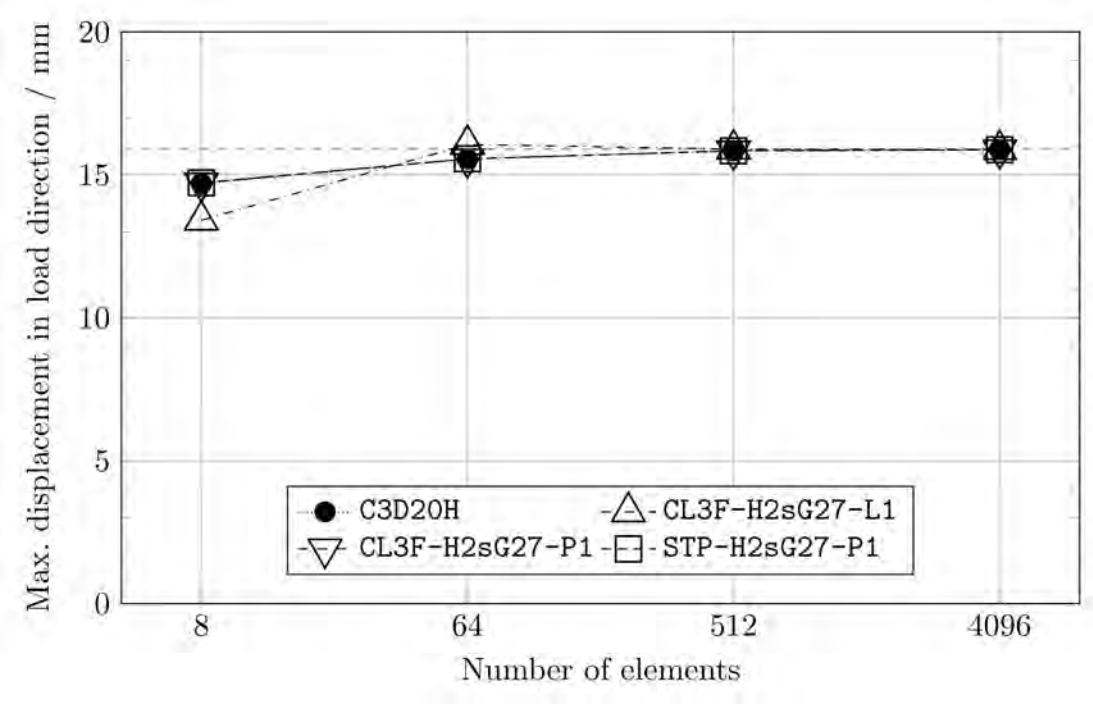

Figure 1: Mesh convergence study: quadratic hexahedral elements

the continuous elements need significantly less equilibrium iterations than the discontinuous elements in general.

The similarity in the mesh convergence behavior for the discontinuous `STP-` and `CL3F-` elements was expected since the semi-discretization approach eliminates variables from the weak form so that we did not expect pronounced differences for converged (i.e. equilibrium) states. However, due to the differences in the tangent stiffness matrix and right-hand side the elements differ in terms of the numerical stability. Under numerical stability (or robustness) we understand the maximum load-step size that can be applied (for a specific combination of hybrid-element and material model) so that the (only locally converging) Newton-Raphson scheme still converges. As a benchmark test we increase the total load, which is always applied in five equidistant steps, until for one of the five load steps the equilibrium iterations diverge. The maximum load for each combination of hybrid element and material model is displayed in Figure 2. It should be mentioned at this point, that a stability benchmark like this is in contrast to mesh convergence studies not at all a standard test in the literature, although the ability to apply large load-steps is obviously a desirable property.

In Abaqus only the standard compression model is readily available. Therefore, in combination with the standard compression model we tested the Abaqus elements (in red) twice: In combination with the internal material model and with the same material model implemented by a `UMAT`. (The nonstandard models are both implemented by `UMAT`s for the testing of the Abaqus hybrid elements.) Interestingly, the internal standard model performs slightly better than the `UMAT` implementation. Comparing only `UMAT` implementations, the Abaqus elements perform worse for compression models with stronger nonlinearity. Especially for the Hartmann-Neff model, the stable step-width of the Abaqus elements is significantly reduced. The original (not augmented) `STP`-elements (in gray) perform worse than the Abaqus elements and suffer from severe stability issues in general. In contrast, the (not augmented) `CL3F`-elements (in blue) perform better than the Abaqus hybrid elements in general. Furthermore, in contrast to the Abaqus elements, all `CL3F`-elements achieve the same stable step-width (within the margin of error of the test) independent of the used compression model. In turn, the advantage of

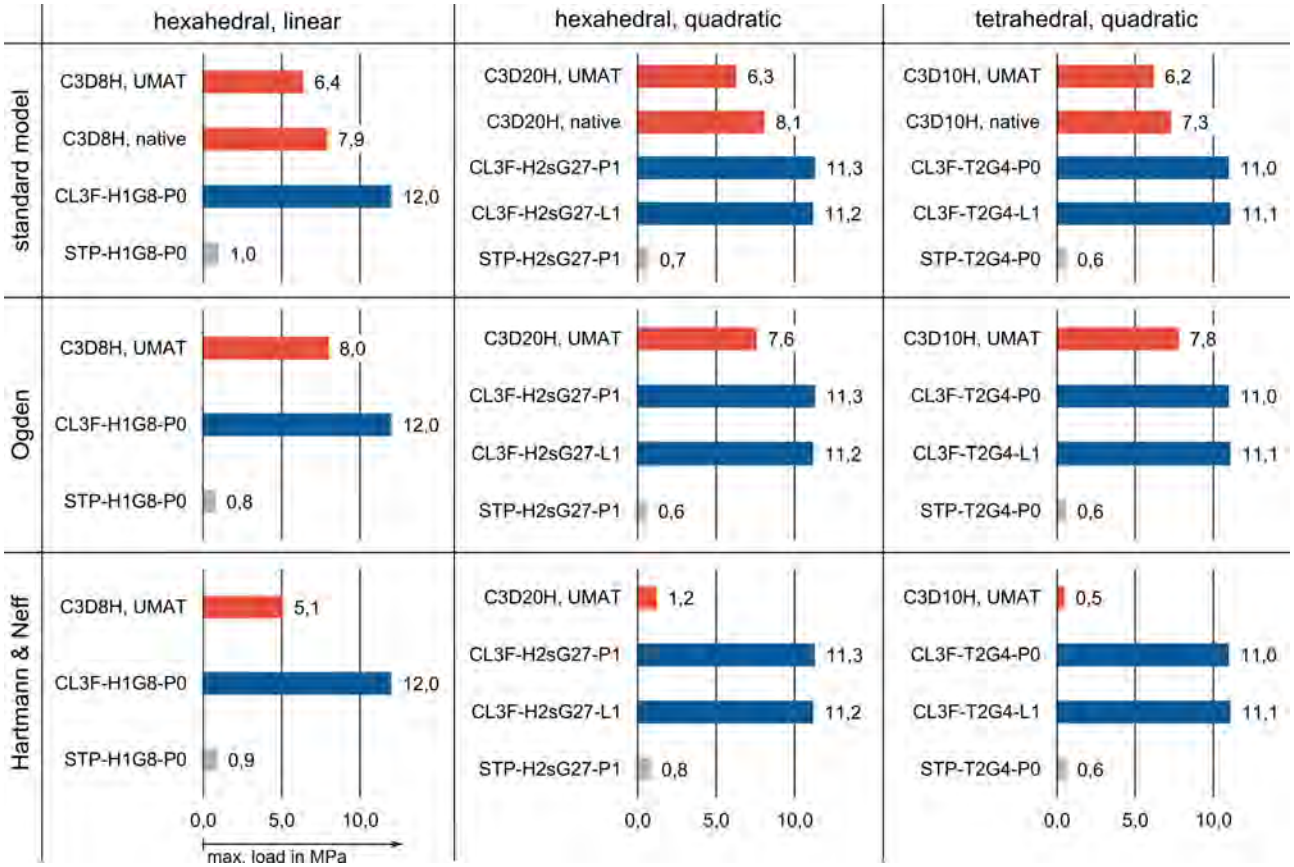

Figure 2: Numerical stability benchmark

the CL3F-elements is huge for the strongly nonlinear Hartmann-Neff model. (Here, the stable step-width is up to 22 times larger.) Another observation is that within the margin of error, we observe no difference in terms of the numerical stability between continuous CL3F-elements and comparable discontinuous CL3F-elements.

5 CONCLUSIONS

Comparing the Abaqus hybrid elements to the STP- and CL3F-elements it should be emphazized that the Abaqus/Standard default settings, especially the default extrapolation was used for the Abaqus hybrid elements, i.e. a method to determine the first guess to the incremental solution. In contrast the initial value of the incremental solution for the implementation of the STP- and CL3F-elements was simply zero. Also, no stabilization techniques were used for the STP- and CL3F-elements. Hence, the Abaqus hybrid elements (which are used as provided) have a huge advantage in the stability benchmark. Therefore, it is remarkable that the CL3F-elements overcome the stability issues of the STP-elements to an extend that they outperform the production stage Abaqus elements, especially since recent hybrid-element formulations often rely heavily on matching numerical stabilization techniques.

REFERENCES

[1] Hartmann, S. and Neff, P., Polyconvexity of generalized polynomial-type hyperelastic strain energy functions for near-incompressibility. *International Journal of Solids and Structures*, Vol. **40**, pp. 2767–2791, (2003).

[2] Ogden, R.W., Large deformation isotropic elasticity - on the correlation of theory and experiment for incompressible rubberlike solids. *Proceedings of the Royal Society A: Math-*

ematical, Physical and Engineering Sciences, Vol. **326**, pp. 565–584, (1972).

[3] Ricker, A., Fehse, A., Kröger, N. H. *Final report on IGF project No. 19916 N, characterization and modeling of compression moduli of technical rubber materials*, 2020. (in German)

[4] Simo, J.C., Taylor, R.L. and Pister, K.S., Variational and projection methods for the volume constraint in finite deformation elasto-plasticity. *Computer Methods in Applied Mechanics and Engineering*, Vol. **51**, pp. 177–208, (1985).

[5] Simo, J.C. and Taylor, R.L., Quasi-incompressible finite elasticity in principal stretches. continuum basis and numerical algorithms. *Computer Methods in Applied Mechanics and Engineering*, Vol. **85**(3), pp. 273–310, (1991).

[6] Simulia, *Abaqus 6.14 theory guide*, Dassault Systèmes Simulia Corp., section 3.2.3., (2014).

[7] Schönherr, J.A., Schneider P. and Mittelstedt, C., Robust hybrid/mixed finite elements for rubber-like materials under severe compression. Submitted to *Computational Mechanics*, under review, (2021).

[8] Wriggers, P. *Nonlinear finite element methods.* Springer, 2008.